



Single-Rotor Helicopter Dynamics and Maneuvering Simulation

Belkacem Kada*

Department of Aerospace Engineering, King Abdulaziz University, Jeddah 21589, Saudi Arabia

Email: bkada@kau.edu.sa

Abstract

This paper presents the development and validation of a robust flight dynamics model for simulation of a full-scale single-rotor helicopter dynamics and maneuvering. A minimum-complexity dynamic model is used to compute the aerodynamic forces and moments using trajectory-planning strategy. A high-order sliding mode (HOSM) observer is used as a numerical differentiator for computing time rate changes of longitudinal and lateral control inputs to the main rotor dynamics during maneuvering. The HOSM differentiator suppresses numerical instability and increases computation accuracy of both dynamic and kinematic characteristics. Using available data and flight test results for UH-60 helicopter, the control input characteristics are interpolated versus flight speeds. A pull-up maneuver is simulated to demonstrate the effectiveness of the proposed model.

Keywords: Helicopter dynamics; Helicopter maneuvering; High-order sliding mode observer; Model-based motion simulation; Single-rotor helicopter; UH-60 helicopter.

1. Introduction

Helicopter dynamics analysis and motion simulation require a consistent dynamic model that would mimic the airframe behavior in response to control inputs. Dynamic modeling of flying vehicles is a central element in the design of flight control systems (FCSs) and motion equations constitute one of the main building blocks of the stability and control loop.

* Corresponding author.

Over the last decades, an increasable effort has been done towards developing model-based helicopter FCSs [1-7] and several successful attempts have been made to design model-based helicopter motion simulators [8-13]. The motivation behind this trend is to achieve an accurate dynamics simulation and design enhanced FCSs. Achievement of multirole missions or flying in adverse conditions demand accomplishment of advanced flight modes, which requires high-fidelity dynamic model for flying qualities assessment. Such modes include vertical take-off and landing, rate command, transitional rate command, and attitude command–attitude hold [14,15]. Flying at extreme conditions such as high rotary speed can result in unpleasant aerodynamic and structural implications such as flutter, swing, dynamic stall, and shock wave [16-22]. The aforementioned issues render the modeling of full-scale helicopter dynamics more challenging and requiring not only appropriate modeling methodologies but also advanced numeric techniques to ensure the robustness, improve the effectiveness, and reduce the computational cost of the formulated models. Many existing models use complex expressions of aerodynamic characteristics and coefficients with huge number of parameters and solve differential equations via conventional numerical methods [23-31]. This usually yields inflexibility, delays, high-cost computations, and numerical instabilities that would result in serious control design issues, restrained handling qualities, and restricted of applicability. To provide concise, robust, and low-cost computation dynamic model, a suitable modeling framework is developed in this paper. The framework integrates the minimum-complexity model (MCM) for a single-rotor helicopter developed by NASA [32] and high-order sliding mode (HOSM) differentiator. The MCM incorporates all the forces and moments contributions from the airframe parts, assumes rigid rotor blades, and uses simplified aerodynamic curves. The HOSM differentiator uses the concept of virtual relative degree to achieve high-precision numerical integration [33]. The rest of the paper is organized as follows. Section 2 presents the modeling of a full-scale single-rotor helicopter kinematics and dynamics using the decomposition approach. In section 3, the control system is described, control input channels are interpolated as function of flight speeds from available real-time tests, and numerical integration via classical and modern algorithms is illustrated. In order to validate the model and show its effectiveness, a pull-up maneuver is simulated in section 4 where non-windy and windy flights are considered. Section 5 gives conclusion and recommendation for the presented work.

2. Helicopter Nonlinear Dynamics Modelling

The helicopter dynamics are formulated by considering that the airframe is a fully articulated rotors system with rigid blades having only the flap degree-of-freedom.

2.1 Helicopter Nonlinear Dynamics

In an inertial-axis system $\{x, y, z\}$ with x - z -plane of symmetry, a six-degree equations of motion model is presented in this section. With x, y, z being helicopter airframe inertial positions and, $\phi(\text{roll}), \theta(\text{pitch}), \psi(\text{yaw})$ its attitudes, the nonlinear model of the single-rotor helicopter system is given as follows.

Force equations

$$\begin{Bmatrix} \dot{u} \\ \dot{v} \\ \dot{w} \end{Bmatrix} = - \begin{Bmatrix} wq - vr \\ ur - wp \\ vp - uq \end{Bmatrix} - g \begin{Bmatrix} \sin \theta \\ \cos \theta \sin \phi \\ \cos \theta \cos \phi \end{Bmatrix} + \frac{1}{m} \begin{Bmatrix} X \\ Y \\ Z \end{Bmatrix} \quad (1)$$

Moment equations

$$\begin{Bmatrix} \dot{p} \\ \dot{q} \\ \dot{r} \end{Bmatrix} = \begin{Bmatrix} (I_{zz}L^* + I_{xz}N^*) / (I_{xx}I_{zz} - I_{xz}^2) \\ [M + (I_{zz} - I_{xx})rp + I_{xz}(r^2 - p^2)] / I_{yy} \\ (I_{xz}L^* + I_{xx}N^*) / (I_{xx}I_{zz} - I_{xz}^2) \end{Bmatrix} \quad (2)$$

with

$$\begin{cases} L^* = L + (I_{yy} - I_{zz})qr + I_{xz}pq \\ N^* = N + (I_{xx} - I_{yy})pq - I_{xz}qr \end{cases}$$

Navigation equations

$$\begin{cases} \dot{x} = uC\theta C\psi + v(S\phi S\theta C\psi - C\phi S\psi) + w(C\phi S\theta C\psi + S\phi S\psi) \\ \dot{y} = uC\theta S\psi + v(S\phi S\theta S\psi + C\phi C\psi) + w(C\phi S\theta S\psi - S\phi C\psi) \\ \dot{h} = uS\theta - vS\phi C\theta + wC\phi C\theta \end{cases} \quad (3)$$

Euler rotations

$$\begin{cases} \dot{\phi} = p + \tan \theta (qS\phi + rC\phi) \\ \dot{\theta} = qC\phi - rS\phi \\ \dot{\psi} = (qS\phi + r\cos \phi) / \cos \theta \end{cases} \quad (4)$$

where 'S' and 'C' denote sine and cosine functions, respectively. In the body-axes reference system, X, Y, Z denote the aerodynamics forces; L, M, N denote the aerodynamic moments; u, v, w , denote the translation velocities; p, q, r denote the roll, pitch, and yaw angular rates; $\dot{x}, \dot{y}, \dot{z}$ denote the inertial linear velocities and g is the gravitational force.

2.2 Total Helicopter Forces and Moments

The total forces $\mathbf{f} = [X \ Y \ Z]^T$ and moments $\mathbf{m} = [L \ M \ N]^T$ acting on the helicopter airframe are computed by summing the forces and moments from its main components as follows,

$$\mathbf{f} = \mathbf{f}_{mr} + \mathbf{f}_{tr} + \mathbf{f}_w + \mathbf{f}_{fus} + \mathbf{f}_{ht} + \mathbf{f}_{vt} \quad (5)$$

$$\mathbf{m} = \mathbf{m}_{mr} + \mathbf{f}_{mr} \times \mathbf{R}_{mr} + \mathbf{f}_{tr} \times \mathbf{R}_{tr} + \mathbf{f}_w \times \mathbf{R}_w + \mathbf{f}_{ht} \times \mathbf{R}_{ht} + \mathbf{f}_{vt} \times \mathbf{R}_{vt} \quad (6)$$

with the subscripts ‘ mr ’, ‘ tr ’, ‘ w ’, ‘ fus ’, ‘ ht ’, and ‘ vt ’ denote the main rotor, tail rotor, wing, fuselage, horizontal tail, and vertical tail, respectively. Neglecting the effect of the rotor downwash, the contribution of the different components are given, in simplified forms, as follows.

2.2.1 Main rotor

$$\mathbf{f}_{mr} = \begin{Bmatrix} X_{mr} \\ Y_{mr} \\ Z_{mr} \end{Bmatrix} = \begin{Bmatrix} -T_{mr} \sin(\delta_{long}) \\ T_{mr} \sin(\delta_{lat}) \\ -T_{mr} \cos(\delta_{long}) \cos(\delta_{lat}) \end{Bmatrix} \quad (7)$$

$$\mathbf{m}_{mr} = \begin{Bmatrix} L_{mr} \\ M_{mr} \\ N_{mr} \end{Bmatrix} = \begin{Bmatrix} Y_{mr} h_{hub} + S_{mr} \delta_{lat} \\ Z_{mr} d_{hub} - X_{mr} h_{hub} + S_{mr} \delta_{long} \\ -Y_{mr} d_{hub} + \tau_{mr} \end{Bmatrix} \quad (8)$$

with δ_{long} , δ_{lat} being the longitudinal and lateral tip-path-plane angles, respectively; d_{hub} , h_{hub} , are the diameter and vertical position of the hub, respectively; S_{mr} denotes lumped flapping stiffness, τ_{mr} denotes rotor torque, u is the x-axis airspeed, ρ is the density, and L_s denotes the lift slope.

2.2.2 Tail rotor

$$\mathbf{f}_{tr} = \begin{Bmatrix} X_{tr} \\ Y_{tr} \\ Z_{tr} \end{Bmatrix} = \begin{Bmatrix} 0 \\ T_{tr} \\ 0 \end{Bmatrix} \quad (9)$$

$$\mathbf{m}_{tr} = \begin{Bmatrix} L_{tr} \\ M_{tr} \\ N_{tr} \end{Bmatrix} = \begin{Bmatrix} Y_{tr} h_{tr} \\ -\tau_{tr} \\ -Y_{tr} d_{tr} \end{Bmatrix} \quad (10)$$

The main-rotor and tail-rotor thrusts are computed by iteration using the following expressions

$$T_{mr} = \frac{\pi}{4} r_{mr}^2 \rho L_{s,mr} N_{b,mr} c_{mr} u \Delta u \quad (11)$$

$$T_{tr} = \frac{1}{4} \rho r_{tr}^2 L_{s,tr} N_{b,tr} c_{tr} \Omega_{tr} (v_{trb} - V_{i,tr}) \quad (12)$$

where r_{mr} , c_{mr} , $N_{b,mr}$ denote the radius, chord, and number of blades, of the main rotor, respectively. r_{tr} , c_{tr} , $N_{b,tr}$ denote the radius, chord, and number of blades, respectively. $L_{s,mr}$ and $L_{s,tr}$ are the blade lift curve slopes for the main rotor and tail rotor. v_{trb} and $V_{i,tr}$ denote the y-axis velocity relative to tail rotor blade and the tail rotor induced velocity and Ω_{tr} is the tail rotor angular rate.

2.2.3 Fuselage

$$\mathbf{f}_f = \begin{Bmatrix} X_f \\ Y_f \\ Z_f \end{Bmatrix} = \begin{Bmatrix} \frac{1}{2} \text{sign}(u) \rho C_{dx,f} u^2 \\ \frac{1}{2} \text{sign}(v) \rho C_{dy,f} v^2 \\ \frac{1}{2} \text{sign}(w - V_{i,mr}) \rho C_{dz,f} (w - V_{i,mr})^2 \end{Bmatrix} \quad (13)$$

$$\mathbf{m}_f = \begin{Bmatrix} L_f \\ M_f \\ N_f \end{Bmatrix} = \begin{Bmatrix} X_f h_f \\ Z_f d_f - X_f h_f \\ -Y_f d_f \end{Bmatrix} \quad (14)$$

where $C_{dx,f}$, $C_{dy,f}$, $C_{dz,f}$ denote the fuselage quadratic drag coefficient along x-, y- and z-axis respectively; D_f and h_f are the fuselage horizontal and vertical positions of the aerodynamic center, and $V_{i,mr}$ is the main rotor induced velocity.

2.2.4 Wing

$$\mathbf{f}_w = \begin{Bmatrix} X_w \\ Y_w \\ Z_w \end{Bmatrix} = \begin{Bmatrix} -\frac{1}{2} \rho \left(\frac{1}{\pi b_w^2} (C_{r,w}^2 u^2 + 2C_{r,w} C_{c,w} u w) + C_{c,w}^2 w^2 \right) \\ 0 \\ \frac{1}{2} \rho (C_{r,w} u^2 + C_{c,w} u w) \end{Bmatrix} \quad (15)$$

$$\mathbf{m}_w = \begin{Bmatrix} L_w \\ M_w \\ N_w \end{Bmatrix} = \begin{Bmatrix} 0 \\ Z_w D_w - X_w h_w \\ 0 \end{Bmatrix} \quad (16)$$

where $C_{r,w}$, $C_{c,w}$ being the wing camber-incidence effect, and the horizontal tail circulation effect, respectively; ; D_w and h_w are the wing horizontal and vertical cg positions, respectively.

2.2.5 Horizontal and Vertical tails

$$\mathbf{f}_{ht} = \begin{Bmatrix} X_{ht} \\ Y_{ht} \\ Z_{ht} \end{Bmatrix} = \begin{Bmatrix} 0 \\ 0 \\ \frac{1}{2} \rho (C_{r,ht} u^2 + C_{c,ht} u (w + D_{ht} q)) \end{Bmatrix} \quad (17)$$

$$\mathbf{m}_{ht} = \begin{Bmatrix} L_{ht} \\ M_{ht} \\ N_{ht} \end{Bmatrix} = \begin{Bmatrix} 0 \\ Z_{ht} D_{ht} \\ 0 \end{Bmatrix} \quad (18)$$

with $C_{r,hb}$, $C_{c,hb}$ being the horizontal tail camber-incidence effect, and the horizontal tail circulation effect, respectively; D_{ht} is the horizontal tail ‘cg’ x-axis position.

$$\mathbf{f}_{vt} = \begin{Bmatrix} X_{vt} \\ Y_{vt} \\ Z_{vt} \end{Bmatrix} = \begin{Bmatrix} 0 \\ \frac{1}{2} \rho (C_{r,vt} u^2 + C_{c,vt} u (v - D_{vt} r)) \\ 0 \end{Bmatrix} \quad (19)$$

$$\mathbf{m}_{vt} = \begin{Bmatrix} L_{vt} \\ M_{vt} \\ N_{vt} \end{Bmatrix} = \begin{Bmatrix} Y_{vt} h_{vt} \\ 0 \\ -Y_{vt} D_{vt} \end{Bmatrix} \quad (20)$$

$C_{r,vt}$, $C_{c,vt}$ are the vertical tail camber-incidence effect, and the vertical tail circulation effect, respectively; D_{vt} is the vertical tail cg x-axis position.

2.3 Load factor

The load factor n of the a helicopter airframe is expressed in terms of linear velocities and accelerations measured in the inertial reference. Three forms of the factor n can be measured as follows [34]

$$n_{fp} = \frac{1}{g} \sqrt{\dot{x}^2 + \dot{y}^2 + (\ddot{z} - g)^2} \quad (21)$$

$$n_t = \frac{\ddot{x}\dot{x} + \ddot{y}\dot{y} + \dot{z}(\ddot{z} - g)}{g \sqrt{\dot{x}^2 + \dot{y}^2 + (\dot{z} - g)^2}} \quad (22)$$

$$n_p = \sqrt{n_{fp}^2 - n_t^2} = 1 - \frac{\ddot{z}}{g} \quad (23)$$

where n_{fp} , n_t , n_p denote the flight path, tangential, and normal (lateral) load factors, respectively. The normal load factor is a measure of the vertical acceleration.

3. Control System Design

3.1 Helicopter control system description

It is well known that a standard helicopter airframe is practically controlled through its rotor system that consists of main and tail rotors as shown in Figure 1. The first rotor generates thrust (lift) and translational control while the second one ensures heading control (see Figure 1).

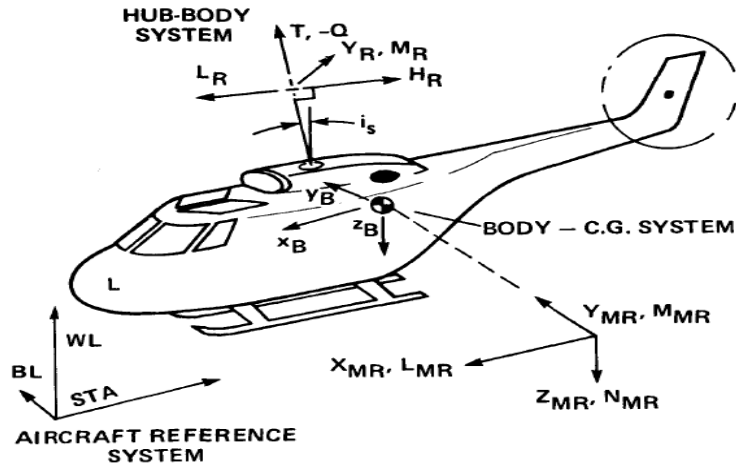
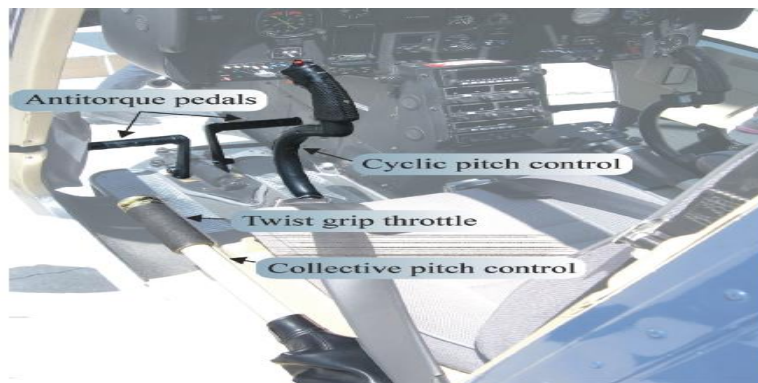
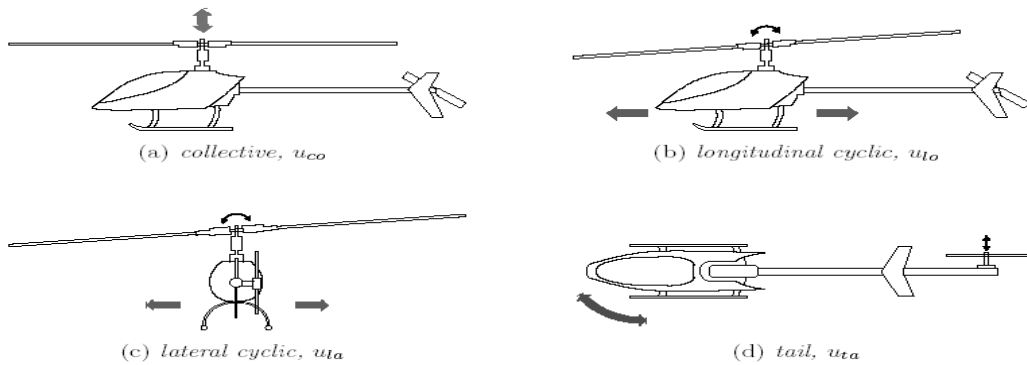


Figure 1: Helicopter rotor system configuration [35]

Hovering, forward flight, and autorotation are the main flight conditions of a helicopter system. To control these flight conditions, a typical flight control system combines four main physical control inputs to achieve different desirable motion modes i.e. collective stick, longitudinal and lateral cyclic sticks, throttle, and directional pedals. Figure2 shows the different controls of a single-rotor helicopter.



(e)

Figure 2: General configuration of a single rotor helicopter flight control system [36]

- *Collective pitch control:* the collective pitch control (CPC) is much more consistent rather than fixed pitch control (FPC) for mid and full size helicopter airframes. CPC is used to control the helicopter airframe at constant speed with variable angle-of-attack (AOA), produce more lift, get very precise and immediate control, perform inverted flight, and get better wind handling immunity. Figure 2a shows the control of the thrust through variation of the collective pitch of the main-rotor blades.
- *Cyclic pitch control:* Cyclic pitch control, often called stick-by-pilot (SBP), is used to change helicopter attitude and airspeed. SBP relieves the helicopter from changing torque spikes and allows avoiding large correction of rotors' speed usually needed in FPC. The longitudinal cyclic control shown in Figure 2b is used to pitch the rotor tip-path plane up or down causing forwards and backwards tilting of the thrust vector in the longitudinal plane. However, the lateral cyclic control shown in Figure 2c rolls the path plane causing right and left tilting of the thrust vector in the lateral plane.
- *Tail rotor control:* Tail rotor control (TRC) or anti-torque pedals are used to increase/decrease the pitch of the tail rotor blades. It also helps compensating for reaction torque produced by the blades' drag or induced by the main rotor. As shown in Figure 2d, the TRC mode is used to control the yaw motion by changing the pitch of the tail rotor blades, which produces change in the magnitude of the balancing torque.
- *Engine Throttle Control:* Engine throttle (ETC) provides the power of helicopter engine. A combination between CPC and ETC is done through an electronic governor to raise the collective pitch lever and increase the pitch.

In terms of input/output, CPC, SBP, TRC, and TRC are the primary control inputs for altitude (all up and all down), attitude (bank left or right, and move forward or aft), heading, and rotor RPM, respectively. Both CPC and ETC are considered as control inputs to the primary force generating rotors. The CPC and TRC are used as control inputs to the primary moment generating rotors. Table 1 lists the aerodynamic control inputs to the helicopter dynamics and shows their corresponding aerodynamic loads [35]

Table 1: Cockpit controls and control phasing

Control	Symbol	Reference	Control axis	Load
Collective Pitch	δ_c	Full down	Heave Control (Up)	+M
Longitudinal cyclic	δ_e	Centered Full-forward	Pitch control (Aft)	+L
Lateral cyclic	δ_a	Centered Full-left	Roll control (Right)	-Z
Directional pedals	δ_p	Centered Full-left	Yaw control	+N

3.2 Helicopter control modelling

The four main control inputs described in Table 1 have been subject to many investigations where different sort

of models have been proposed such as in [35,37]. In this paper, we use an interpolation model that relates the helicopter control inputs to the airframe forward speed V . Using the available data for the UH-60A [37], the following polynomial relationships were obtained

$$\begin{cases} \delta_c = -1.22 \times 10^{-11} V^6 + 5.94 \times 10^{-9} V^5 - 1.12 \times 10^{-6} V^4 + 10.2610^{-5} V^3 - 3.96 \times 10^{-3} V^2 + 10.6 \times 10^{-3} V + 9.0174 \\ \delta_a = 1.85 \times 10^{-9} V^5 - 77.07 \times 10^{-8} V^4 + 11.65 \times 10^{-7} V^3 - 7.32 \times 10^{-3} V^2 + 16.19 \times 10^{-2} V + 3.75 \\ \delta_e = 3.79 \times 10^{-11} V^6 - 2 \times 10^{-8} V^5 + 4.04 \times 10^{-6} V^4 - 3.92 \times 10^{-4} V^3 + 18.34 \times 10^{-3} V^2 - 38.51 \times 10^{-2} V - 0.3013 \\ \delta_p = 1.3 \times 10^{-9} V^5 - 5.11 \times 10^{-7} V^4 + 7.17 \times 10^{-5} V^3 - 3.2 \times 10^{-3} V^2 - 85.63 \times 10^{-3} V + 24.064 \end{cases} \quad (24)$$

The interpolation variance σ^2 and root mean square error μ are as follows

$$\begin{cases} \sigma_{\delta_c}^2 = 0.9995, & \mu = 47.10 \times 10^{-3} \\ \sigma_{\delta_a}^2 = 0.9819, & \mu = 174.21 \times 10^{-3} \\ \sigma_{\delta_e}^2 = 0.9825, & \mu = 391.60 \times 10^{-3} \\ \sigma_{\delta_p}^2 = 0.9969, & \mu = 147.74 \times 10^{-3} \end{cases} \quad (25)$$

Figure 3 shows the change of the UH-60A helicopter control inputs with respect to its flying velocity.

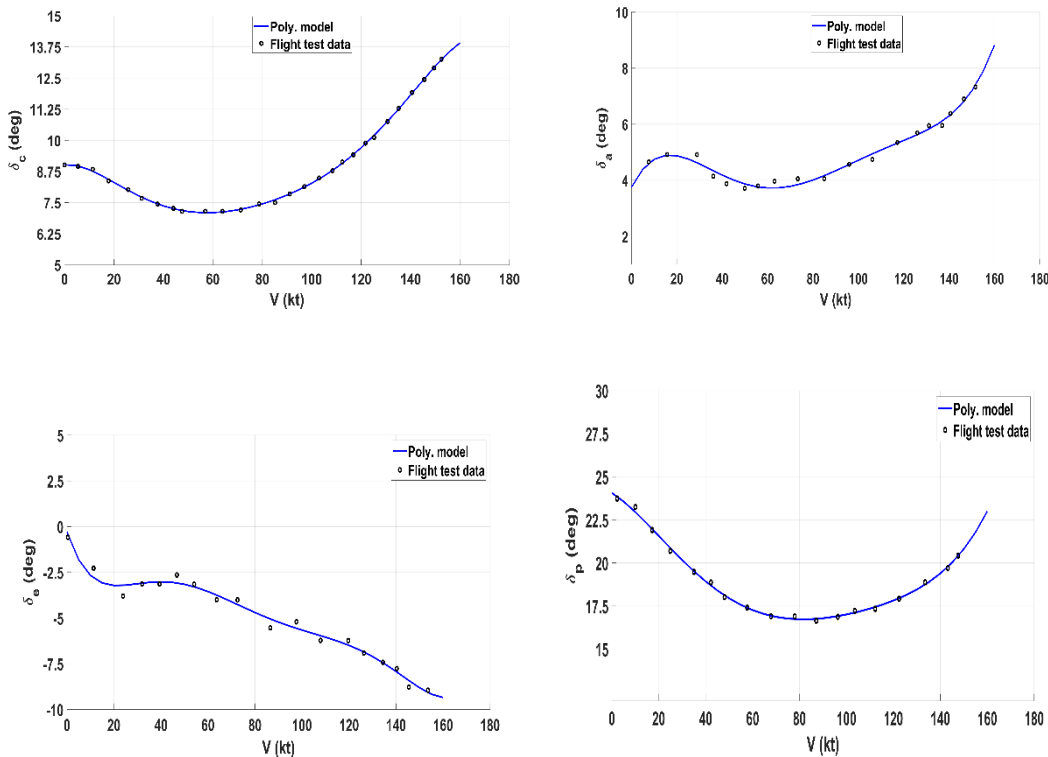


Figure 3: UH-90A control inputs interpolation

The longitudinal and lateral tip-path-plane angles δ_{long} and δ_{lat} affect directly the main rotor forces and moments as shown in equations (5) and (6). Both angles are computed using the following differential models

$$\dot{\delta}_{long} = H(t)\Gamma, \quad \dot{\delta}_{lat} = S(t)\Gamma \quad (26)$$

with

$$H(t) = \chi_{long} - \frac{\omega_y}{\Gamma} - \delta_{long} + \frac{\partial \xi}{\partial u} u, \quad S(t) = \chi_{lat} - \frac{\omega_x}{\Gamma} - \delta_{lat} + \frac{\partial \xi}{\partial v} v, \quad \Gamma = \frac{1}{16} N_{loc} \omega_r \quad (27)$$

where χ_{long} , χ_{lat} are the longitudinal and lateral swashplate angles, respectively; ξ is the lateral flapping and ω_r is the rotor angular rate; u and v are the forward and side components of the velocity vector.

$$\frac{\partial \xi}{\partial u} = \frac{\partial \xi}{\partial v} \left[1 + \frac{3}{2} \frac{u^2}{(r_{mr} \omega_{mr})^2} \right], \quad \frac{\partial \xi}{\partial v} = \frac{8}{3} \frac{\mu_{mr}}{r_{mr} \omega_{mr}} + 2 \frac{(w - V_{i,mr})}{(r_{mr} \omega_{mr})^2} \quad (28)$$

μ_{mr} is the main rotor collective pitch angle. The lock number N_{lock} given as

$$N_{loc} = \frac{\rho a c R^4}{I_b} \quad (29)$$

with a is the slope of the 2D airfoil lift curve, c is the chord length, R is the rotor radius, and I_b is the flapping moment of inertia.

3.3 Numerical Integration

The numerical integration of the expressions (26) is usually performed using the classical two-step Adams-Bashforth technique as shown in the following expression

$$\delta_{long}^{(k+1)} = \delta_{le}^{(k)} + \Delta t \left(a_1 H^{(k)} \Gamma + a_2 H^{(k-1)} \Gamma \right), \quad \delta_{lat}^{(k+1)} = \delta_a^{(k)} + \Delta t \left(a_1 S^{(k)} \Gamma + a_2 S^{(k-1)} \Gamma \right) \quad (30)$$

where Δt denotes the sampling time and a_1, a_2 are numerical integration constants.

The classical Adams-Bashforth integration scheme has shown numerical instability mainly at the presence of perturbations in the initial conditions or starting values [38]. To build a stable solution to the helicopter dynamics problem, we propose the use of the following robust HOSM numerical differentiator [33].

$$\begin{cases} \text{for } k = 0, \dots, r-1 & \text{with } r > 1 \\ \dot{\xi}_k = v_k, & \text{with } v_{-1} = \sigma \\ v_k = -\beta_k L^{r-k} \left| \xi_k - v_{k-1} \right|^{\frac{r-k}{r+1}} \text{sign}(\xi_k - v_{k-1}) + \xi_{k+1} \end{cases} \quad (31)$$

where $\dot{\xi}_k$ ($k = 2, 1, \dots, r-1$) denote the successive time derivatives of the measured signal, observed parameter, or the tracking error σ . β_k denote the differentiator gains and L is a Lipschitz constant. The

coefficient r is the relative degree denoting the higher order time derivative of σ being computed. According to the properties of the HOSM differentiator, at least $r - 1$ of the successive time derivatives are exact. According to the algorithm (31), the first and third order time derivatives of the signal σ are given as follows.

$$\begin{cases} \dot{\xi}_1 = -\beta_1 L |\xi_1 - v_0|^{\frac{1}{3}} \text{sign}(\xi_1 - v_0) + \xi_2 & \text{for } r = 2 \\ \dot{\xi}_2 = -\beta_2 L |\xi_2 - v_1|^{\frac{1}{4}} \text{sign}(\xi_2 - v_1) + \xi_3 & \text{for } r = 3 \end{cases} \quad (32)$$

where ξ_i and v_i are computed using the algorithm (31). One of the advantages of the numerical HOSM differentiator is that the virtual increase of the relative order r yields high-accuracy calculation of the antecedent $r - 1$ time derivatives.

4. Simulation

To evaluate the effectiveness of the proposed control model, a pull-up maneuver scenario is simulated for UH-60A helicopter using the available data in [39]. Pull-up maneuvering is one of the most important motion trajectories of a helicopter to avoid obstacles such as mountains as shown in Figure 4.



Figure 4: A helicopter climbing a mountain [40]

Figure 5 shows a simulated pull-up maneuver with initial forward speed of 46.3 m/s (90 kt) at 1000 m (3,280.85 ft) altitude to avoid a mountain with a height of 2020 m (6627.3 ft).

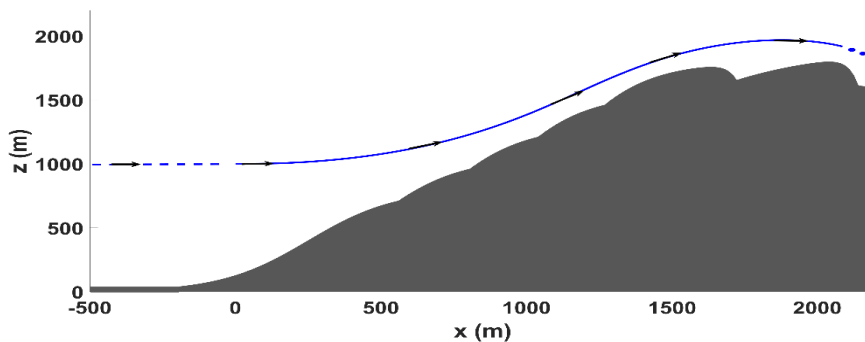


Figure 5: Simulated pull-up maneuver

The maneuver goal consists of reaching an altitude gain of 968 m (3175.85 ft) without exceeding a maximum normal load factor of $n_p = 2.5g$. It is worth noting that according to FAR PART 27 regulations [41], the normal load factor should not exceed a value of $n_{max} = 3.5g$ in order to avoid any structural damage to the helicopter airframe or its components. Since the pull-up maneuver is performed with constant speed V , the airframe velocities vector is given, from equation (3), in the inertial axes as follows

$$\dot{x}_e = V \cos \theta \cos \psi, \quad \dot{y}_e = V \cos \theta \sin \psi, \quad \dot{z}_e = V \sin \theta \quad (33)$$

Figure 6 and Figure 7 depict the time-history of the flight speed u (forward speed) and the normal and longitudinal load factors, respectively. Figure 8 and Figure 9 show the corresponding changes in the vertical aerodynamic z-axis force and pitch moment.

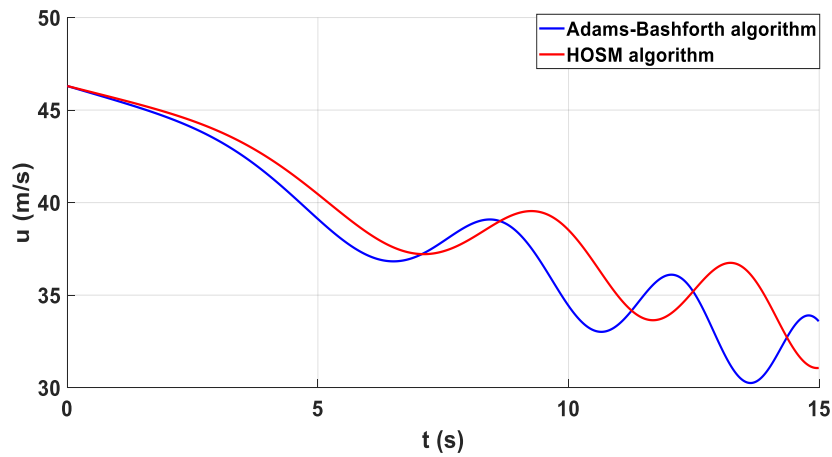


Figure 6: Time-history of the forward speed decay

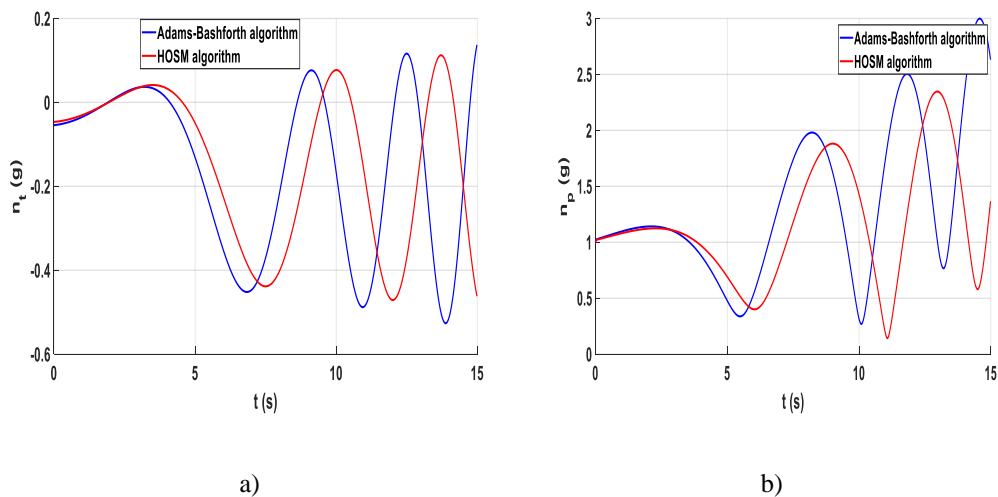


Figure 7: Load factors: a) tangential, b) normal

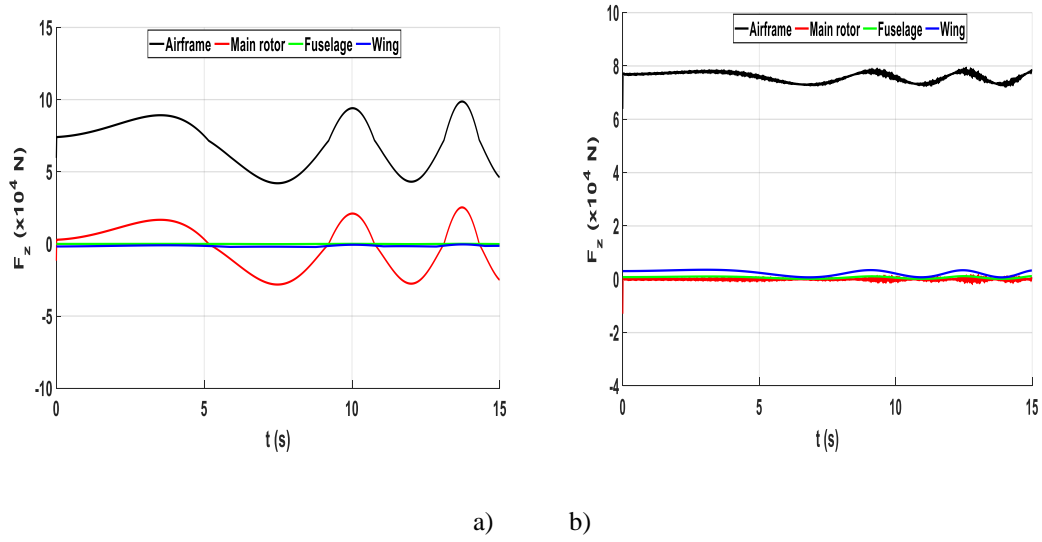


Figure 8: Aerodynamic z-axis force F_z : a) HOSM-based algorithm, b) Adams-Bashforth algorithm,

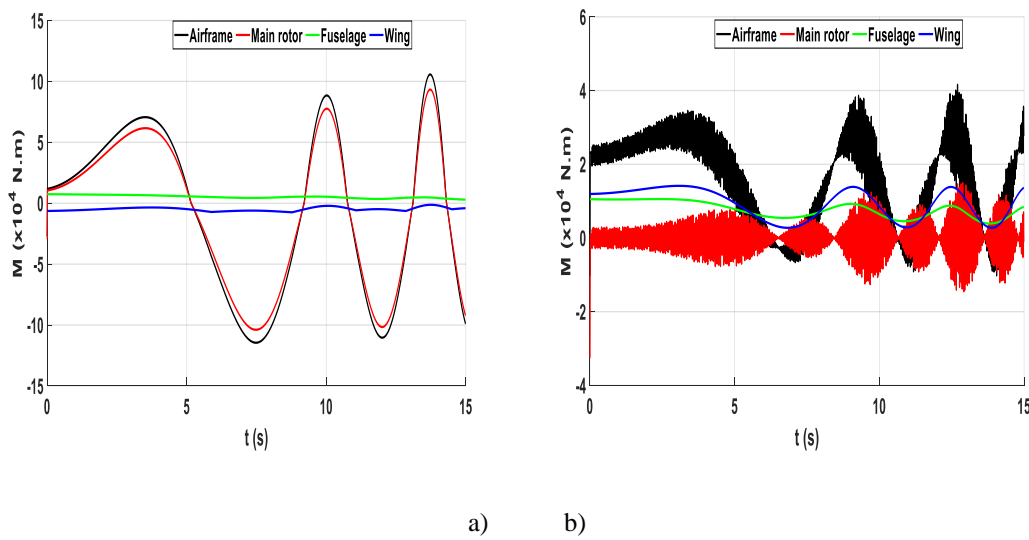


Figure 9: Aerodynamic pitch moment: a) HOSM differentiator, b) Adams-Bashforth differentiator

Table 2: Comparison study of windy and non-windy flights

	HOSM algorithm $u_g=0$	A-B Algorithm	HOSM algorithm $u_g \neq 0$
V_f	31.07 (m/s)	33.60 m(s)	18.16 (m/s)
$n_{p,max}$	2.35 < 2.5 (g)	2.995 > 2.5(g)	2.29 < 2.5(g)
$n_{t,max}$	0.11 (g)	0.134 (g)	0.18
T_{max}	8586 (N.m/s)	15,891(Nm/s)	11,457 (N.m/s)
$F_{z,max}$	98683.80 (N)	17,851 (N)	11,0961 (N)
M_{max}	105,739 (N.m)	3,068.1 (N.m)	145,615 (N.m)

Table 2 summarizes the results of a comparison study between flight in windy and non-windy atmosphere. The non-windy simulation is performed for both HOSM-based and AB-based algorithms. The windy flight is simulated for HOSM-based algorithm with $V_g = [0 \ 0 \ -12.86]^T \text{ m/s } (-25 \text{ kt})$

5. Conclusion

In this paper, a dynamic model for helicopter dynamics and maneuverability simulation has been presented. First, a velocity-based control model was interpolated from exciting experimental data to compute the control inputs to the airframe dynamics as functions of the forward flight speed. Second, a dynamic model was built based upon the contributions of the main components of the vehicle in producing the necessary aerodynamic forces and moment. Due to the numeric instability of the two-step Adams-Bashforth integration algorithm, a high-order sliding mode observer was used as a numerical differentiator to suppress instability and increase accuracy of computations. Simulation results obtained for a pull-up maneuver has shown the effectiveness of the proposed model in achieving mission requirements without overstressing the airframe.

6. Recommendations

Future work will focus on the design of the flight control system based upon the trajectory of the helicopter and its maneuvering. The developed motion-maneuvering model will be integrated in the control loop of full-scale helicopter for development of advanced flight control systems.

Acknowledgment

This article was funded by the Deanship of Scientific Research (DSR), King Abdulaziz University, Jeddah. The author, therefore, acknowledges with thanks DSR technical and financial support.

References

- [1]. A. Isidori, L. Marconi, A. Serrani, "Robust nonlinear motion control of a helicopter," *IEEE Trans. On Autom. Control* vol. 48, no 3, pp. 413–426 2003.
- [2]. E. Prempain and I. Postlethwaite, "Static H_∞ loop shaping control of a fly-by-wire helicopter," *Automatica*, vol. 41, no. 9, pp. 1517–1528, 2005.
- [3]. M.L. Civita., G. Papageorgiou, W.C. Messner, T. Kanade, "Design and flight testing of an H_∞ controller for a robotic helicopter," *Journal of Guidance, Control, and Dynamics*, vol. 29, no. 2, pp. 485–494, 2006.
- [4]. I.A. Raptis, K.P. Valavanis, W.A. Moreno, "A novel nonlinear backstepping controller design for helicopters using the rotation matrix," *IEEE Trans. Control Syst. Technol.*, vol. 19, no. 2, pp. 465–473, 2011.
- [5]. P. Bibik, and J. Narkiewicz, "Helicopter optimal control after power failure using comprehensive dynamic model," *Journal of Guidance, Control and Dynamics*, vol. 35, no. 4, pp. 1354–62, July 1, 2012.
- [6]. T. Ertuğrul, M.A. Adli, and M.U. Salamci, "Model reference adaptive control design for helicopters

- using gain scheduled reference models,” Proceedings of the 17th IEEE International Carpathian Control Conference (ICCC '16), pp. 182–187, Tatranska Lomnica, Slovakia, May 2016.
- [7]. J. Hu, and H. Gu, “Survey on flight control technology for large-scale helicopter,” *International Journal of Aerospace Engineering*, vol. 2017, Article ID 5309403, 14 pages, 2017.
- [8]. S. Klaes, “ATTAS and ACT/FHS system simulation for preflight software and hardware testing,” in Proceedings of the AIAA Modelling and Simulation Technologies Conference and Exhibit, Monterey, Calif, USA, August 2002.
- [9]. D. Yilmaz, and I. Yavrucuk, “Development of a flight dynamics model for a UH-1H helicopter simulator,” Ankara International Aerospace Conference, Ankara, September, 2007.
- [10]. G. Padfield, “Helicopter flight dynamics: the theory and application of flying qualities and simulation modelling,” 2nd edn. Blackwell, Oxford. 2007
- [11]. I. Yavrucuk, E. Kubali, O. Tarimci, and D. Yilmaz, “A low cost flight simulator using virtual reality tools,” American Institute of Aeronautics and Astronautics, Modelling and Simulation Technologies Conference, Chicago, Illinois, August, 2009.
- [12]. A.S. Royer, A.J. Doud, M.L. Rose, B. He, “EEG control of a virtual helicopter in 3-dimensional space using intelligent control strategies,” *IEEE Transactions on neural systems and rehabilitation engineering*, vol.18, no. 6, 2010, pp. 581-9
- [13]. B. Kada, “Helicopter nonlinear dynamics modelling for motion simulation and real-time control”, 10th International Conference on Advances in Engineering and Technology (AET-18), Malaysia, 2018
- [14]. B.J. Baskett, “Aeronautical design standard performance specification handling qualities requirements for military rotorcraft,” Tech. Rep. ADS-33E-PRF, Army Aviation and Missile Command, Redstone Arsenal, Ala, USA, 2000.
- [15]. J. Hu and H. Gu , “Survey on Flight Control Technology for Large-Scale Helicopter”, *International Journal of Aerospace Engineering*, vol. 2017, Article ID 5309403, 2017.
- [16]. B. Haycock, and P. Grant, “A real-time helicopter model with flexible main rotor blades,” AIAA Modelling and Simulation Technologies Conference, Portland, Oregon, August 2011.
- [17]. N.G. Marichal, M. Tomas-Rodriguez, A. Lopez, S. Castillo-Rivera, and P. Campoy, “Vibration reduction for vision system on board uav using a neuro-fuzzy controller,” *Journal of Vibration and Control*, 2012.
- [18]. D., Liu, J., Xin, and J., Huang, “The theoretical research for the rotor/fuselage unsteady aerodynamic interaction problem,” *Journal of Aerospace Technology and Management*, vol. 8, no. 3, pp. 281-288, 2016.
- [19]. A. Choudhry, R. Leknys, M. Arjomandi, and R. Kelso, “An insight into the dynamic stall lift characteristics,” *Exp. Therm. Fluid Sci.* vol. 58, pp. 188–208, 2016.
- [20]. S. Guntur, N.N. Sørensen, S. Schreck, and L. Bergami, “Modelling dynamic stall on wind turbine blades under rotationally augmented flow fields,” *Wind Energy*, vol. 19, pp. 383–397, 2016.
- [21]. M.R. Amoozgar, H. Shahverdi, and A.S. Nobari. "Aeroelastic stability of hingeless rotor blades in hover using fully intrinsic equations", *AIAA Journal*, vol. 55, no. 7, pp. 2450-2460, 2017.
- [22]. K.V. Truong, “Modelling aerodynamics, including dynamic stall, for comprehensive analysis of helicopter rotors,” *Aerospace*, vol. 4, no. 21, 2017.

- [23]. W. Johnson, "Helicopter theory," Princeton University Press, Princeton 1980.
- [24]. R. DuVal, "A real-time multi-body dynamics architecture for rotorcraft simulation: the challenge of realistic rotorcraft simulation," RAES Conference, pp. 9.1–9.12, November 7–9, 2001.
- [25]. A. Bramwell, G. Done, and D. Balmford, "Bramwell's helicopter dynamics," 2nd ed., Butterworth Heinemann, Oxford, UK, 2001.
- [26]. J. Leishman, "Principles of helicopter aerodynamics," 2nd Ed., Cambridge University Press, New York, NY, 2006.
- [27]. D.G. Padfield, "Helicopter flight dynamics: the theory and application of flying qualities and simulation modelling," 2nd ed., Blackwell Publishing, Oxford, UK, 2007.
- [28]. B. Aponso, D. Tran, and J. Schroeder, "Rotorcraft research at the NASA vertical motion simulator," Proceedings of the American Helicopter Society 64th Annual Forum, vol. 63, p. 2390, Montreal, Canada, April 2008.
- [29]. A. Punjani and P. Abbeel, "Deep learning helicopter dynamics models," IEEE International Conference on Robotics and Automation (ICRA) Washington State Convention Center Seattle, Washington, May 26-30, 2015
- [30]. K.V. Truong, "Modelling aerodynamics for comprehensive analysis of helicopter rotors," In Proceedings of the 42nd European Rotorcraft Forum, Lille, France, 5–8 September 2016.
- [31]. B. Lawrence, T. Berger, and M.B. Tischler, "Integrating flight dynamics & control analysis and simulation in rotorcraft conceptual design," Proceedings of the American Helicopter Society 72nd Annual Forum, West Palm Beach, Fla, USA, May 2016.
- [32]. P. Talbot, B. Tinling, W. Decker, and R. Chen, "A mathematical model of a single main rotor helicopter for piloted simulation", Tech. rep., NASA TM 84281, 1982
- [33]. A. Levant, "Higher-order sliding modes, differentiation and output-feedback control", International Journal of Control, 2003, Vol. 76, no 9/10, pp. 924–941
- [34]. K. Ferguson, and D. Thomson, Maneuverability assessment of a compound helicopter configuration, Journal of the American Helicopter Society, vol. 61, no. 1, pp. 1-15, 2016.
- [35]. P.D. Talbot, B.E. Tinling, W.A. Decker, and R.T. N. Chen, "A Mathematical Model of a Single Main Rotor Helicopter for Piloted Simulation", NASA Technical Memorandum 84281, 1982.
- [36]. K. Volkov, Flight Physics - Models, Techniques and Technologies, chapter 2, IntechOpen, 2018, ISBN: 978-953-51-3808-2
- [37]. K. Ferguson, D. Thomson, and D. Anderson, "Investigation of a Compound Helicopter Flying the Depart and Abort Mission Task Element", Presented at the AHS Rotorcraft Handling Qualities, Huntsville, Alabama, 2017
- [38]. E. Süli, and D. Mayers, "An Introduction to Numerical Analysis", Cambridge University Press, 2003, ISBN 0-521-00794-1.
- [39]. K.B. Hilbert, "A Mathematical Model of the UH-60 Helicopter", NASA Technical Memorandum 85890, 1984.
- [40]. <https://unsplash.com/photos/SveC4JcxGrM>
- [41]. <http://www.aviation-safety-bureau.com/federal-aviation-regulations.html>